

Generation of Terawatt Attosecond Pulses from Relativistic Transition Radiation

Xinlu Xu^{1,*}, David B. Cesar,¹ Sébastien Corde^{1,2}, Vitaly Yakimenko,¹ Mark J. Hogan,¹ Chan Joshi,³ Agostino Marinelli,^{1,†} and Warren B. Mori^{3,4}

¹SLAC National Accelerator Laboratory, Menlo Park, California 94025, USA

²LOA, ENSTA Paris, CNRS, Ecole Polytechnique, Institut Polytechnique de Paris, 91762 Palaiseau, France

³Department of Electrical Engineering, University of California, Los Angeles, California 90095, USA

⁴Department of Physics and Astronomy, University of California Los Angeles, Los Angeles, California 90095, USA



(Received 25 July 2020; revised 4 November 2020; accepted 29 January 2021; published 2 March 2021)

When a femtosecond duration and hundreds of kiloampere peak current electron beam traverses the vacuum and high-density plasma interface, a new process, that we call relativistic transition radiation (RTR), generates an intense ~ 100 as pulse containing ~ 1 terawatt power of coherent vacuum ultraviolet (VUV) radiation accompanied by several smaller femtosecond duration satellite pulses. This pulse inherits the radial polarization of the incident beam field and has a ring intensity distribution. This RTR is emitted when the beam density is comparable to the plasma density and the spot size much larger than the plasma skin depth. Physically, it arises from the return current or backward relativistic motion of electrons starting just inside the plasma that Doppler up shifts the emitted photons. The number of RTR pulses is determined by the number of groups of plasma electrons that originate at different depths within the first plasma wake period and emit coherently before phase mixing.

DOI: 10.1103/PhysRevLett.126.094801

Transition radiation (TR) is a well-known phenomenon that happens when charged particles traverse an interface between two different media [1]. Electrons contained in the two media respond differently to the electric field carried by the charged particles and this leads to the emission of TR. An important case of TR happens when relativistic charged particles propagate across a vacuum-plasma or vacuum-metal foil interface. In this scenario, electrons on the surface move in response to the transverse electric field of the beam, forming a surface current that screens the field and, in the process, emits radiation. For wavelengths longer than the bunch duration, the emitted photons are coherent, and the radiated pulse typically has a time structure similar to the bunch current profile. Therefore, coherent transition radiation is widely used to diagnose the longitudinal profile of (sub)picosecond electron beams [2–9], as well as to produce intense terahertz radiation using kiloampere current beams with subpicosecond duration [10–12]. If the bunch duration is shorter than the plasma oscillation period, then a wake is excited and a train of pulses will be generated [13,14] at the boundary between a plasma or foil with a vacuum or neutral gas after the initial transition radiation.

Attosecond pulse generation has attracted much interest during the past two decades driven by its ability to resolve the electronic motion on the atomic scale [15–24]. In this Letter, we describe a new regime of TR which can generate a high power attosecond pulse that is accompanied by several smaller amplitude pulses separated by $\sim 2\pi c/\omega_p$ due to the unique beam-plasma dynamics that results when

the surface electrons move relativistically. This regime leads to some unique features of the radiation such as radial polarization [25] and a narrow ring intensity distribution. The dominant attosecond pulse generated with this method could be synchronized with synchrotron or free-electron laser radiation emitted by the same electron bunch, therefore making possible x-ray pump-probe experiments with unprecedented accuracy. Alternatively, one could separate the long-wavelength oscillations from the short attosecond burst with a frequency filter (or a thin foil), and combine them on a target for pump-probe or strong-field experiments.

This new regime of TR can now be accessed because high brightness electron beams produced by state-of-the-art photoinjectors can generate beams which have space-charge/Coulomb fields ranging from GV/m to TV/m [26–29]. Such large fields can in turn accelerate free electrons in the vicinity of the beam to relativistic energies during the transit time of the beam [30]. However, even for such beam intensities, when the plasma density is greater than the beam density ($n_p \gg n_b$) the motion of electrons is nonrelativistic due to the shielding effect of the free electrons and standard TR still occurs.

This new process, which we call relativistic transition radiation (RTR), happens when the plasma electrons move relativistically. To understand the physics of RTR it is useful to recall the normalized parameters that are used when describing plasma wakefield acceleration in the blowout regime [31,32]. Consider a bi-Gaussian beam, $n_b = n_{b0} \exp(-(r^2/2\sigma_r^2) - (z^2/2\sigma_z^2))$, and the parameter

$\Lambda \equiv n_{b0}/n_p (k_p \sigma_r)^2 \equiv k_{pb}^2 \sigma_r^2$, where $k_{p,pb} \equiv \omega_{p,pb}/c$ and $\omega_{p,pb}$ is the plasma frequency using either the plasma or beam density, respectively. In the relativistic blowout regime $\Lambda > 1$ and the spot size of the beam is kept much less than a skin depth (equivalently when $n_{b0} \gg n_p$) and $k_p \sigma_z \sim 1$. Under these conditions the electrons move relativistically in response to the unshielded electric field of the beam. A nonlinear wakefield is produced and the currents from these wakes radiate from the boundary through a nonlinear mode conversion process [13,14]. This radiation tends to be long wavelength and weak for wavelengths shorter than the plasma oscillation period. However, RTR occurs if the spot size for the same beam (with $\Lambda \gg 10$) is increased such that it is comparable to the blowout radius $2\sqrt{\Lambda}k_p^{-1}$ or equivalently when $n_{b0} \sim n_p$.

Under these heretofore unexplored conditions, a large number of plasma electrons are pushed predominately forward rather than blown out, which leads to a new regime of TR with multiple pulses. They are pushed outward by the radial electric field of the beam and then gain forward velocity through the magnetic field, i.e., the $v \times B$ force. As the plasma electrons are displaced forward, they leave a positive charge density behind which, in turn, excites strong return currents. If the return electrons reach relativistic energies they emit strongly Doppler-shifted radiation in the backward direction, giving rise to short radiation pulses. The first (we call zeroth) pulse is radiated by the forward current and has characteristics similar to traditional TR where the electric field is in the opposite direction to the beam's field, but its duration is longer than the bunch duration. However, there are subsequent pulses arising from the backward motion of electrons (return current now flows within the beam) arising deeper inside the plasma but from a region with thickness smaller than the wavelength of the first plasma wake. The most intense pulse is composed of photons that are Doppler up shifted by the backward motion of the most energetic return current relativistic electrons. This results in radiation that has frequency components significantly higher than the natural plasma frequency. Particle-in-cell (PIC) simulations show one of the radiated pulses can be as short as 100 as with terawatt-level peak power by using femtosecond, ultrahigh-current electron bunches envisioned for the next generation of plasma-wakefield experiments [29].

To demonstrate the physics behind RTR and how it generates an isolated attosecond pulse, 3D fully relativistic PIC simulations are performed with the code OSIRIS [33]. We use bi-Gaussian beams and the simulations use normalized units. However, in what follows the actual beam parameters correspond to 6.5×10^9 electrons and $\sigma_r = 1.5 \mu\text{m}$ and $\sigma_z = 0.4 \mu\text{m}$ to make connections to possible near-term experiments [29]. This corresponds to $n_{b0} = 3.7 \times 10^{20} \text{ cm}^{-3}$, a peak current of $I = 250 \text{ kA}$, and a skin depth for the beam density of $c/\omega_{pb} = 0.28 \mu\text{m}$. As

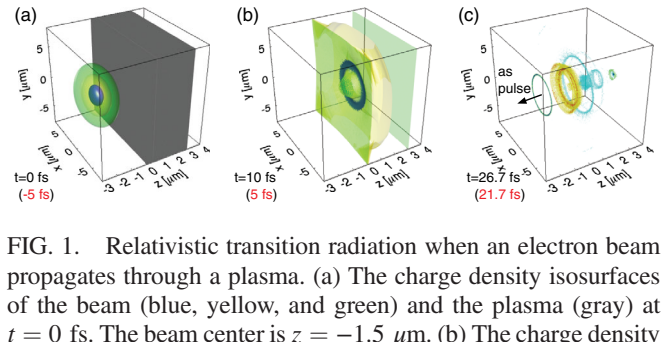


FIG. 1. Relativistic transition radiation when an electron beam propagates through a plasma. (a) The charge density isosurfaces of the beam (blue, yellow, and green) and the plasma (gray) at $t = 0 \text{ fs}$. The beam center is $z = -1.5 \mu\text{m}$. (b) The charge density isosurface of the plasma electrons at $t = 10 \text{ fs}$. (c) The isosurfaces of the radiated transverse electric field E_{\perp} (green and blue) and the axial current j_z (red and yellow represent forward current density while cyan represents the backward current density) at $t = 26.7 \text{ fs}$. Red times are relative to the time when the middle of the beam hits the surface.

depicted in Fig. 1(a), a 10 GeV electron beam propagates into a cold plasma with immobile ions that exists between the $z = 0 \mu\text{m}$ and $z = 3 \mu\text{m}$. When $n_p \gg n_{b0}$ and $k_p \sigma_r \gg 1$, the space-charge field and current are screened in a distance much less than the beam spot size so that well-known nonrelativistic TR (non-RTR) happens. In the opposite limit, where $n_p \ll n_{b0}$ and $k_p \sigma_r \ll 1$, the plasma electrons within a radius much larger than the beam spot size move relativistically outward and forward [32]. These sheath electrons are then pulled backward with relativistic energies, and this process is what sets up wakefields inside the plasma, provided the plasma is many skin depths long.

However, when the plasma density and beam density are both high and roughly equal to one another, plasma electrons that start inside and outside the beam can be accelerated to relativistic energies without a large transverse displacement. For the bi-Gaussian charge distribution of the beam electrons, plasma electrons initially at $r_i \sim 1.5\sigma_r$ experience the strongest space-charge field, $E_r \approx cB_{\theta} \approx 0.45(n_{b0}e\sigma_r/\epsilon_0)\exp(-(z^2/2\sigma_z^2))$, and acquire the largest axial speeds, while electrons with $r_i \gg \sigma_r$ or $r_i \ll \sigma_r$ are pushed forward less significantly. Thus, a region void of plasma electrons forms at the surface whose shape can be approximated as a hollow cylinder, with an annular cross section [Fig. 1(b)] in r and a thickness d (in z) is formed. The thickness can be estimated by balancing the forward force ($v_r/cB_{\theta} \sim E_r$) on plasma electrons from the beam with the charge separation force. If we further assume that $d \lesssim \sigma_r$, then the longitudinal field can be estimated from a one-dimensional argument as $n_e ed/2\epsilon_0$; thus the thickness can be obtained by balancing this with the force from the beam pushing electrons forward,

$$\frac{n_p ed}{2\epsilon_0} \sim 0.45 \frac{n_{b0} e \sigma_r}{\epsilon_0} \rightarrow d \sim \frac{n_{b0}}{n_p} \sigma_r, \quad (1)$$

which is close to the $1 \mu\text{m}$ observed in simulations. This large surface electric field then pulls electrons initially

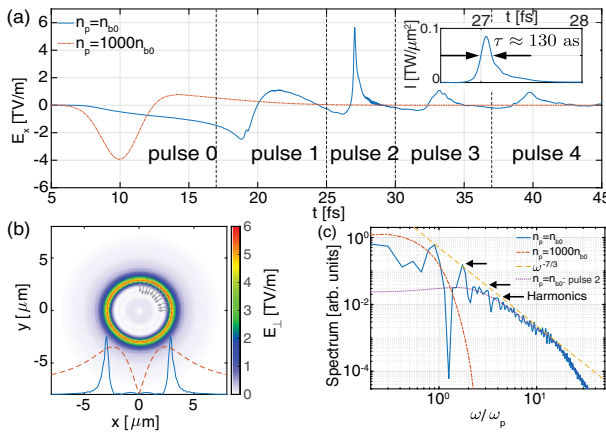


FIG. 2. Attosecond radiation pulse. (a) The recorded electric field when $n_p = n_{b0}$ (blue curve) and $1000n_{b0}$ (red curve). Normalized intensity profile of the radiation (pulse 2) is shown in the inset. (b) The distribution of the transverse electrical field in the x - y plane at $t = 27.1$ fs and $z = -1.5$ μm . The gray arrows indicate the direction of the field. The solid blue line shows the field amplitude at $y = 0$ μm and the dashed red line is for magnitude of the incident Coulomb field. (c) The spectrum of the radiation when $n_p = n_{b0}$ (blue line), $1000n_{b0}$ (red line), the fitted scaling law (yellow line), and the pulse 2 when $n_p = n_{b0}$ (purple line).

located deeper in the plasma backward. These electrons are then accelerated backward toward and across the boundary and they emit radiation we refer to as RTR. The work done by the charge separation force on these backward moving plasma electrons can be estimated using a one-dimensional argument as

$$\Delta W \approx \int_d^0 dz \frac{-e^2 n_p (d-z)}{2\epsilon_0} = \frac{m_e c^2}{4} (k_p d)^2, \quad (2)$$

which is $\sim 3m_e c^2$ if using $d \approx 1$ μm . Simulations show one intense attosecond pulse is emitted along the $-z$ direction which is compressed due to the relativistic Doppler effect [Fig. 1(c)]. There is some forward radiation as well, but it is not as short nor intense as the backward one. Depending on the thickness of the target, this process can recur several times and produce several somewhat broader pulses with the energy in the later pulses progressively decreasing as phase mixing of electron oscillations occurs.

The detailed characteristics of the radiation from this RTR are shown in Fig. 2. The time profiles of the transverse electric field at a fixed location ($z = -1.5$ μm , $x = -2.95$ μm , $y = 0$ μm) are presented in Fig. 2(a) for RTR ($n_p = n_{b0}$) and non-RTR ($n_p = 1000n_{b0}$). The radiation E_x emanating from the high-density plasma (red curve) is approximately proportional to the incident space-charge fields. In the RTR case, there is a pulse with the electric field direction similar to the higher-density case between 5 and 17 fs for the RTR (pulse 0, blue curve). The second (pulse 2, blue curve) and most prominent pulse has a half-cycle profile with very short,

130 as, duration (FWHM of the intensity) and a large peak electric field, 5.66 TV/m, which is even larger than the incident space-charge field (4.5 TV/m). The intensity profile of the pulse 2 is shown in the inset. The transverse cross section of the attosecond pulse has an annular shape with 0.27 μm width (solid blue) which is much smaller than the 3.6 μm width of the space-charge field (dashed red line). The radiation is radially polarized as indicated by the gray arrows in Fig. 2(b). The peak power is 0.74 TW and the energy contained in pulse 2 is 0.15 mJ. The transverse mode and the polarization of the radiation is inherited from the incident morphology of the space-charge field. Thus, a transversely asymmetric driver can be used to control the distribution and the polarization of the attosecond pulse [34]. The attosecond pulse generation is relatively insensitive to the exact density profile, thickness, and initial temperature of the plasma. A thicker target which can support multiple wake periods has little effect on the emission of RTR (see Movies M1–M3 in Supplemental Material [30]). Simulations described in the Supplemental Material show if the plasma temperature is increased to as high as 1 keV the attosecond pulse is still present. If the initial plasma temperature is less than 10 eV and an up-ramp has a characteristic length less than 200 nm radiation pattern changes little. Simulations with moving hydrogen or carbon ions give similar attosecond pulses (see Supplemental Material [30]).

We compare the spectrum of the radiation from RTR and non-RTR in Fig. 2(c). The spectrum from non-RTR is mainly from the incident beam that decays quickly (red dotted line) after $\omega \sim c/\sigma_z \approx \omega_p$, while the one from RTR extends to much higher frequencies because of the relativistic Doppler shift of the photons emitted by the backward moving electrons. This broad spectrum of the radiation extends up to $\omega \approx 18\omega_p$ and provides the broad bandwidth needed to support the highest power, attosecond pulse. The central frequency of the photons in this ultra-short pulse is 7 eV, which is in the VUV region. Harmonics of the nonlinear plasma oscillation are observed since one pulse is radiated from each plasma period. The ratio of the intensity between each peak shown in Fig. 2(a) is 0.19:0.038:1:0.037:0.028 [35].

The details of the plasma response and surface currents generated by high current beams with $n_p = n_{b0}$ crossing a sharp interface are very complicated. This is illustrated by examining the current carried by the plasma electrons that start within $\sim 2\pi k_p^{-1}$ (or 1.7 μm) of the surface; these currents are the source of the radiation and all the properties of the radiation can be traced back to the motion of these electrons. The longitudinal and transverse current distributions at four different times (t_{rad}) when the RTR pulses are emitted [Fig. 2(a)] are shown in Fig. 3(a). Since electrons close to the surface emit the RTR, we identify a group of electrons that form the current (white dots in j_x plots) and trace their trajectories backward. The initial positions of each group of these electrons are shown in Fig. 3(b). The first group

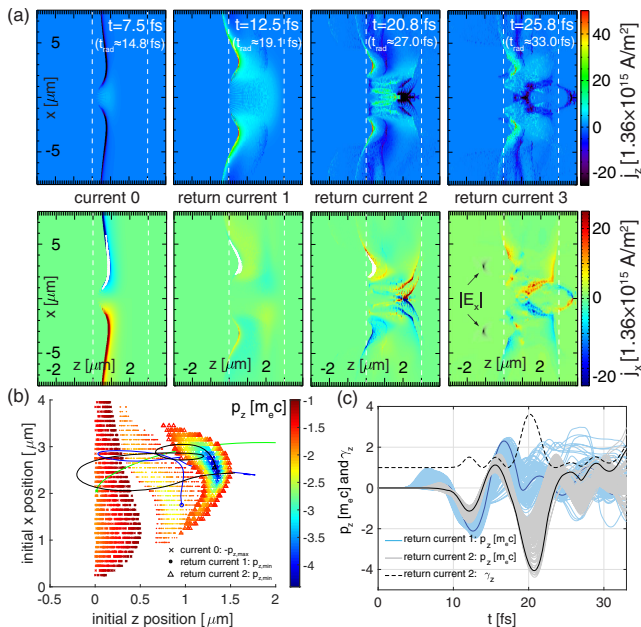


FIG. 3. The motion of plasma electrons. (a) The x - z plane distribution of the longitudinal (j_z) and transverse (j_x) current densities at four different times (t). The radiation generated at these times will arrive at the recorded position at t_{rad} . The dashed lines indicate the two boundaries of the target. The field distribution of the attosecond pulse (gray) is also shown in the last j_x plot. (b) The initial positions of the electrons in three groups indicated by crosses, dots, and triangles originating at different locations within the target determine the source of the current densities that radiates the zeroth, first, and second electromagnetic pulse. The positions of each group of electrons when they coalesce into a high-density current sheath are shown as white dots in the corresponding j_x plots of (a). Also shown are sample trajectories of three of these electrons (see also Movies M4–M6 in Supplemental Material [30]). (c) The evolution of p_z for the electrons in return currents. The solid lines represent two sample electrons and the black dashed line shows the γ_z of one sample from return current 2.

[crosses in Fig. 3(b)] is called current 0 because these electrons are mostly pushed forward by beam. When the beam enters the plasma its radial electric field first pushes them outward and, once they acquire relativistic energies, forward by the magnetic field of the beam (see Supplemental Material, Movie M4 [30]) as represented by the trajectory of one representative electron (green) shown in this figure. Trajectory crossing of electrons from this group starting at different axial positions occurs and these electrons coalesce into similar axial positions leading to a high-density current sheet as shown in first column of Fig. 3(a). The transverse components of these currents generate pulse 0 [5–17 fs in Fig. 2(a)].

After the driver passes, electrons that started deeper inside the plasma [dots in Fig. 3(b)], and that were overtaken by the first group of electrons closer to the surface, and hence accelerated by the fields of the beam less significantly, now move radially into the region of the strong fields within the

hollow cylinder and are then accelerated backward. Thus, a forward flowing current distribution (return current 1) is formed as shown in the second column of Fig. 3(a) and gives rise to the radiated pulse 1 [17–25 fs in Fig. 2(a)]. These backward flowing electrons then cross into the vacuum. A sheath field is generated at the boundary that then pulls them back into the plasma (see the blue representative trajectory) where they are met by a group of electrons that started with axial positions slightly even deeper in the plasma [triangles in Fig. 3(b)]. The forward moving electrons pass through the second group of return current electrons, causing the second group of electrons to be further accelerated backward, thus forming return current 2. This second group thus has higher energies than the first group as seen in their current distribution shown in the third column of Fig. 3(a). Intense attosecond pulse [25–30 fs in Fig. 2(a)] is emitted by this high-density return current sheath. This mixing of the trajectories of electrons that started at different axial positions leads to several bursts of the return current before the entire process phase mixes away. The return current formed by the third group is shown in the fourth column of Fig. 3(a). At this time, the radiated attosecond pulse has already moved away from the rear surface.

The axial momentum of the electrons in the return currents are shown in Fig. 3(c). The electrons in return current 1 (dots) achieve a maximum backward momentum $\sim 2m_ec$ around $t \sim 12$ fs. As a comparison, the electrons in return current 2 (triangles) achieve even larger backward momentum $\sim 4m_ec$ around $t \sim 20$ fs. Compared with a relativistic plasma mirror, the electrons here only achieve the maximum backward momentum during a short time. And this “ γ -spike” effect leads to a further reduction of the radiated pulse duration [36]. A crude estimation of the radiation pulse duration can be given as $\tau \sim \tau_{\gamma_z}/2\gamma_z^2 \approx 3 \text{ fs}/2 \times 4^2 \approx 100 \text{ as}$, where τ_{γ_z} is the duration of the γ spike.

When the electron driver is incident obliquely upon the target with a small angle, the radiation is produced approximately along the direction of specular reflection. The pulse produced by the return current 2 is shown in

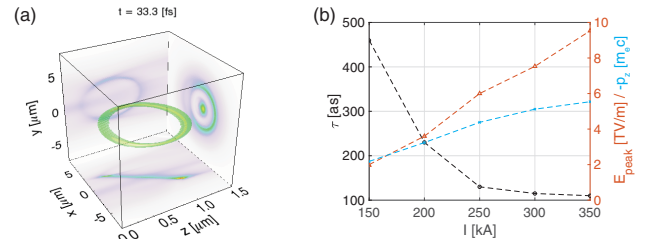


FIG. 4. (a) The isosurface of the radiation intensity (yellow, $E^2 = 50(m^2c^2\omega_p^2/e^2)$; green, $E^2 = 30m^2c^2\omega_p^2/e^2$) and its projections in each plane when the beam propagates along the z direction and the target is oblique in the z - x plane with angle $\theta = 5.7^\circ$. (b) The duration, peak electric field of the attosecond pulse, and the maximum backward momentum of the electrons when scanning the current of the normally incident beam.

Fig. 4(a) for an angle of incidence of $\theta = 5.7^\circ$. In Fig. 4(b), we show how the maximum backward momentum of the electrons in return current 2 and the duration and the peak field of the attosecond pulse is affected by the peak current of the electron beam. When the peak density (and current) of a beam with fixed charge (0.84 nC) and $1.5 \mu\text{m}$ spot size is increased, the maximum backward momentum of electrons increases, and the duration of the attosecond pulse decreases and the field amplitude increases. The density of the plasma is also higher, as it is always set equal to the peak density of the beam to ensure an efficient generation of attosecond pulse.

In conclusion, using 3D PIC simulations we have demonstrated that relativistic transition radiation is generated when a high current relativistic electron beam propagates through a plasma with $n_{b0} \sim n_p$. For realizable experimental parameters, the radially polarized radiation has a ring intensity distribution, is more intense in the backward direction, and contains a ~ 1 terawatt, ~ 100 as pulse flanked by several smaller femtosecond pulses.

This work was supported by the U.S. Department of Energy under DOE Award No. DE-AC02-76SF00515, the Department of Energy Basic Energy Sciences accelerator and detector research program FWP 100497, DOE Award No. DE-SC0010064, and SciDAC FNAL subcontract 644405, and NSF Grants No. 1806046 and No. 1734315, and the European Research Council (ERC) under the European Union's Horizon 2020 research and innovation programme (Miniature beam-driven Plasma Accelerators project, Grant Agreement No. 715807). The simulations were performed on the UCLA Hoffman 2 and Dawson 2 Clusters, and the resources of the National Energy Research Scientific Computing Center (NERSC), a U.S. Department of Energy Office of Science User Facility located at Lawrence Berkeley National Laboratory.

- [7] Y. Glinec, J. Faure, A. Norlin, A. Pukhov, and V. Malka, *Phys. Rev. Lett.* **98**, 194801 (2007).
- [8] O. Lundh, C. Rechatin, J. Lim, V. Malka, and J. Faure, *Phys. Rev. Lett.* **110**, 065005 (2013).
- [9] T. J. Maxwell, C. Behrens, Y. Ding, A. S. Fisher, J. Frisch, Z. Huang, and H. Loos, *Phys. Rev. Lett.* **111**, 184801 (2013).
- [10] W. P. Leemans, C. G. R. Geddes, J. Faure, C. Tóth, J. van Tilborg, C. B. Schroeder, E. Esarey, G. Fubiani, D. Auerbach, B. Marcelis, M. A. Carnahan, R. A. Kaindl, J. Byrd, and M. C. Martin, *Phys. Rev. Lett.* **91**, 074802 (2003).
- [11] D. Daranciang, J. Goodfellow, M. Fuchs, H. Wen, S. Ghimire, D. A. Reis, H. Loos, A. S. Fisher, and A. M. Lindenberg, *Appl. Phys. Lett.* **99**, 141117 (2011).
- [12] Z. Wu, A. S. Fisher, J. Goodfellow, M. Fuchs, D. Daranciang, M. Hogan, H. Loos, and A. Lindenberg, *Rev. Sci. Instrum.* **84**, 022701 (2013).
- [13] H. Hamster, A. Sullivan, S. Gordon, W. White, and R. W. Falcone, *Phys. Rev. Lett.* **71**, 2725 (1993).
- [14] Z.-M. Sheng, H.-C. Wu, K. Li, and J. Zhang, *Phys. Rev. E* **69**, 025401(R) (2004).
- [15] P. Gibbon and A. R. Bell, *Phys. Rev. Lett.* **68**, 1535 (1992).
- [16] F. Quéré, C. Thaury, P. Monot, S. Dobosz, P. Martin, J.-P. Geindre, and P. Audebert, *Phys. Rev. Lett.* **96**, 125004 (2006).
- [17] P. B. Corkum and F. Krausz, *Nat. Phys.* **3**, 381 (2007).
- [18] F. Krausz and M. Ivanov, *Rev. Mod. Phys.* **81**, 163 (2009).
- [19] U. Teubner and P. Gibbon, *Rev. Mod. Phys.* **81**, 445 (2009).
- [20] C. Thaury and F. Quéré, *J. Phys. B* **43**, 213001 (2010).
- [21] D. An der Brügge and A. Pukhov, *Phys. Plasmas* **17**, 033110 (2010).
- [22] B. Dromey, S. Rykov, M. Yeung, R. Hörlein, D. Jung, D. Gautier, T. Dzelzainis, D. Kiefer, S. Palaniyppan, R. Shah *et al.*, *Nat. Phys.* **8**, 804 (2012).
- [23] H.-C. Wu, J. Meyer-ter Vehn, J. Fernández, and B. M. Hegelich, *Phys. Rev. Lett.* **104**, 234801 (2010).
- [24] H.-C. Wu and J. Meyer-ter Vehn, *Nat. Photonics* **6**, 304 (2012).
- [25] Q. Zhan, *Adv. Opt. Photonics* **1**, 1 (2009).
- [26] I. Blumenfeld *et al.*, *Nature (London)* **445**, 741 (2007).
- [27] J. P. MacArthur, J. Duris, Z. Zhang, A. Lutman, A. Zholents, X. Xu, Z. Huang, and A. Marinelli, *Phys. Rev. Lett.* **123**, 214801 (2019).
- [28] J. Duris, S. Li, T. Driver, E. G. Champenois, J. P. MacArthur, A. A. Lutman, Z. Zhang, P. Rosenberger, J. W. Aldrich, R. Coffee *et al.*, *Nat. Photonics* **14**, 30 (2020).
- [29] V. Yakimenko, L. Alsberg, E. Bong, G. Bouchard, C. Clarke, C. Emma, S. Green, C. Hast, M. J. Hogan, J. Seabury, N. Lipkowitz, B. O'Shea, D. Storey, G. White, and G. Yocky, *Phys. Rev. Accel. Beams* **22**, 101301 (2019).
- [30] See Supplemental Material at <http://link.aps.org/supplemental/10.1103/PhysRevLett.126.094801> for more details.
- [31] J. B. Rosenzweig, B. Breizman, T. Katsouleas, and J. J. Su, *Phys. Rev. A* **44**, R6189 (1991).
- [32] W. Lu, C. Huang, M. Zhou, W. B. Mori, and T. Katsouleas, *Phys. Rev. Lett.* **96**, 165002 (2006).
- [33] R. Fonseca *et al.*, *Lect. Notes Comput. Sci.* **2331**, 342 (2002).

*xuxinlu@slac.stanford.edu
†marinelli@slac.stanford.edu

- [1] V. Ginzburg and I. Frank, *Zh. Eksp. Teor. Fiz.* **9**, 353 (1945) [*J. Phys. USSR* **9**, 353 (1945)].
- [2] U. Happek, A. J. Sievers, and E. B. Blum, *Phys. Rev. Lett.* **67**, 2962 (1991).
- [3] Y. Liu, X. J. Wang, D. B. Cline, M. Babzien, J. M. Fang, J. Gallardo, K. Kusche, I. Pogorelsky, J. Skaritka, and A. van Steenbergen, *Phys. Rev. Lett.* **80**, 4418 (1998).
- [4] A. Tremaine, J. B. Rosenzweig, S. Anderson, P. Frigola, M. Hogan, A. Murokh, C. Pellegrini, D. C. Nguyen, and R. L. Sheffield, *Phys. Rev. Lett.* **81**, 5816 (1998).
- [5] A. H. Lumpkin, R. Dejus, W. J. Berg, M. Borland, Y. C. Chae, E. Moog, N. S. Sereno, and B. X. Yang, *Phys. Rev. Lett.* **86**, 79 (2001).
- [6] J. van Tilborg, C. B. Schroeder, C. V. Filip, C. Tóth, C. G. R. Geddes, G. Fubiani, R. Huber, R. A. Kaindl, E. Esarey, and W. P. Leemans, *Phys. Rev. Lett.* **96**, 014801 (2006).

[34] The properties of the radiation when using transversely asymmetric electron beams are discussed in Supplemental Material [30].

[35] For example, the intensity ratio is 0.033:0.006:1:0.01:0.006 after a numerical filter with form $\exp[-(\omega/\omega_p - 50/46)^{10}]$ is used and the pulse 2 acquires a duration of 88 as and a peak electric field of 3.2 TV/m.

[36] T. Baeva, S. Gordienko, and A. Pukhov, *Phys. Rev. E* **74**, 046404 (2006).